Structural insights into the Slit-Robo complex

Cecile Morlot*, Nicole M. Thielens†, Raimond B. G. Ravelli*, Wieger Hemrika‡, Roland A. Romijn‡, Piet Gros§, Stephen Cusack*, and Andrew A. McCarthy*¶

*European Molecular Biology Laboratory, 6 Rue Jules Horowitz, BP 181, 38042 Grenoble, France; †Laboratoire d'Enzymologie Moleculaire, Institut de Biologie Structurale J. P. Ebel, 38027 Grenoble Cedex 1, France; and ‡ABC Expression Center and §Department of Crystal and Structural Chemistry, Bijvoet Center for Biomolecular Research, Utrecht University, Padualaan 8, 3584 CH Utrecht, The Netherlands

Edited by Corey S. Goodman, Renovis, South San Francisco, CA, and approved August 7, 2007 (received for review June 6, 2007)

Slits are large multidomain leucine-rich repeat (LRR)-containing proteins that provide crucial guidance cues in neuronal and vascular development. More recently, Slits have been implicated in heart morphogenesis, angiogenesis, and tumor metastasis. Slits are ligands for the Robo (Roundabout) receptors, which belong to the Ig superfamily of transmembrane signaling molecules. The Slit-Robo interaction is mediated by the second LRR domain of Slit and the two N-terminal Ig domains of Robo, but the molecular details of this interaction and how it induces signaling remain unclear. Here we describe the crystal structures of the second LRR domain of human Slit2 (Slit2 D2), the first two Ig domains of its receptor Robo1 (Ig1–2), and the minimal complex between these proteins (Slit2 D2-Robo1 Ig1). Slit2 D2 binds with its concave surface to the side of Ig1 with electrostatic and hydrophobic contact regions mediated by residues that are conserved in other family members. Surface plasmon resonance experiments and a mutational analysis of the interface confirm that Ig1 is the primary domain for binding Slit2. These structures provide molecular insight into Slit-Robo complex formation and will be important for the development of novel cancer therapeutics.

guidance cues | neurons | signaling

Bilaterally symmetric nervous systems, such as those of insects and vertebrates, possess a special midline structure that establishes a partition between the left and right mirror-image halves. To connect and coordinate both sides, a subset of so-called commissural axons has to cross the midline. Developing commissural axons navigate through the embryo by processing and responding to a number of different signals in their immediate environment. Both Slit and Netrin and their receptors, Roundabout (Robo) and Deleted in Colorectal Carcinoma (DCC), provide key ligand–receptor interactions for this process during neuronal development, especially at the midline of the central nervous system of vertebrates and invertebrates (1, 2). The Slit-Robo signaling complex is also central to the development of blood vessels (3, 4) and some organs, for example, the heart (5, 6). In addition, Slit2 has been implicated in breast cancer metastasis (7) and Robo1 in heptacellular carcinoma (8).

Three Slit proteins (Slit1–3) (9) and four Robo proteins (Robo1, Robo2, Robo3/Rig-1, and the vascular-specific Robo4/magic Roundabout) (10–12) have been identified in mammals. Netrin and Slit1–3 are secreted by the midline cells, whereas DCC and Robo1–3 are expressed on the surface of growing axons (2). During neuronal development, the commissural axons are initially attracted to the midline through a Netrin–DCC-mediated interaction (2). This attractive signal is subsequently silenced near the midline to allow crossing through a Slit-mediated interaction between DCC and Robo (13). Slit-Robo signaling then induces repulsion, expelling the axons from the midline and preventing recrossing (1). In vertebrates, Robo3 is also proposed to have a role in midline crossing by antagonizing Robo1 (14). The exact details of this mechanism remain unknown, but two Robo3 isoforms (Robo3A and Robo3B) that differ only at their N terminus by alternative splicing have recently been identified (15). These studies show that, although the Robo3A isoform is unable to bind Slit2, it can still form heterophilic interactions with Robo1. This raises the possibility that Robo3 may, in fact, sequester Robo1 into an inactive receptor complex on the developing axon to allow midline crossing (15).

Slit proteins contain a unique N-terminal tandem of four leucine-rich repeat (LRR) domains (D1–D4) followed by seven to nine EGF-like domains, a laminin G domain and a C-terminal cysteine-rich module (16). Proteolytic cleavage within the EGF region releases the active N-terminal fragment (17). The ectodomain of Robo1–3 consists of five Ig-like (Ig1–Ig5) and three type III fibronectin domains (18), whereas Robo4 has only two Ig domains. Slits1–3 cross-interact with Robo1–3 via their second LRR domain and first two Ig domains, respectively (19, 20). However, the binding partner(s) for Robo4 still remains unclear. Heparin has also been observed to bind Slit2 and is proposed to form an integral component of the Slit-Robo signaling complex (21). The crystal structure of the third LRR domain of *Drosophila* Slit (dSlit D3) has been determined (20), and elsewhere, we describe the crystal structure of the equivalent domain of Slit2 (Slit2 D3) (22), which has one more LRR than dSlit D3. To help elucidate the exact molecular basis of Slit-Robo signaling, we biochemically characterized and determined the structures of the separate interacting domains of human Robo1 and Slit2, as well as the minimal complex between them. These studies reveal that Ig1 of Robo1 is the primary interaction domain for Slit2, and that the bipartite interaction region involves highly conserved residues from both proteins.

Results

Structure of Robo1 Ig1-2. The crystal structure of the first two Ig domains from human Robo1 was determined at 2.5-Å resolution by using the multiple wavelength anomalous diffraction technique from a single mercury derivative (Table 1). Both domains have the canonical I1 β-sandwich fold formed by two antiparallel β-sheets containing strands ABB′ED and strands A′GG′FCC′ and an internal disulfide bridge connecting βF to the linker between βB and βB′ (23) (Fig. 1*A*). The closest structural neighbors to Ig1 and Ig2 are the Ig domains 1 and 4, respectively, of the chicken neural axonin-1 (24) ($rmsd_{92C\alpha}$ = 1.1 Å and $rmsd_{89C\alpha}$ = 1.5 Å). There is essentially no polypeptide linker between the two domains, the final strand of Ig1 (βG′) being

Author contributions: C.M., S.C., and A.A.M. designed research; C.M., N.M.T., R.B.G.R., W.H., R.A.R., and A.A.M. performed research; W.H., R.A.R., and P.G. contributed new reagents/analytic tools; C.M., N.M.T., S.C., and A.A.M. analyzed data; and C.M., S.C., and A.A.M. wrote the paper.

The authors declare no conflict of interest.

This article is a PNAS Direct Submission.

Freely available online through the PNAS open access option.

Abbreviations: SPR, surface plasmon resonance; LRR, leucine-rich repeat.

Data deposition: The atomic coordinates and structure factors have been deposited in the Protein Data Bank, www.pdb.org [PDB ID codes 2v9q (Robo1 Ig1-2; crystal form 1), 2v9r (Robo1 Ig1-2; crystal form 2), 2v9s (Slit2 D2), and 2v9t (Slit2 D2-Robo1 Ig1)].

¶To whom correspondence should be addressed. E-mail: andrewmc@embl.fr.

This article contains supporting information online at www.pnas.org/cgi/content/full/0705310104/DC1.

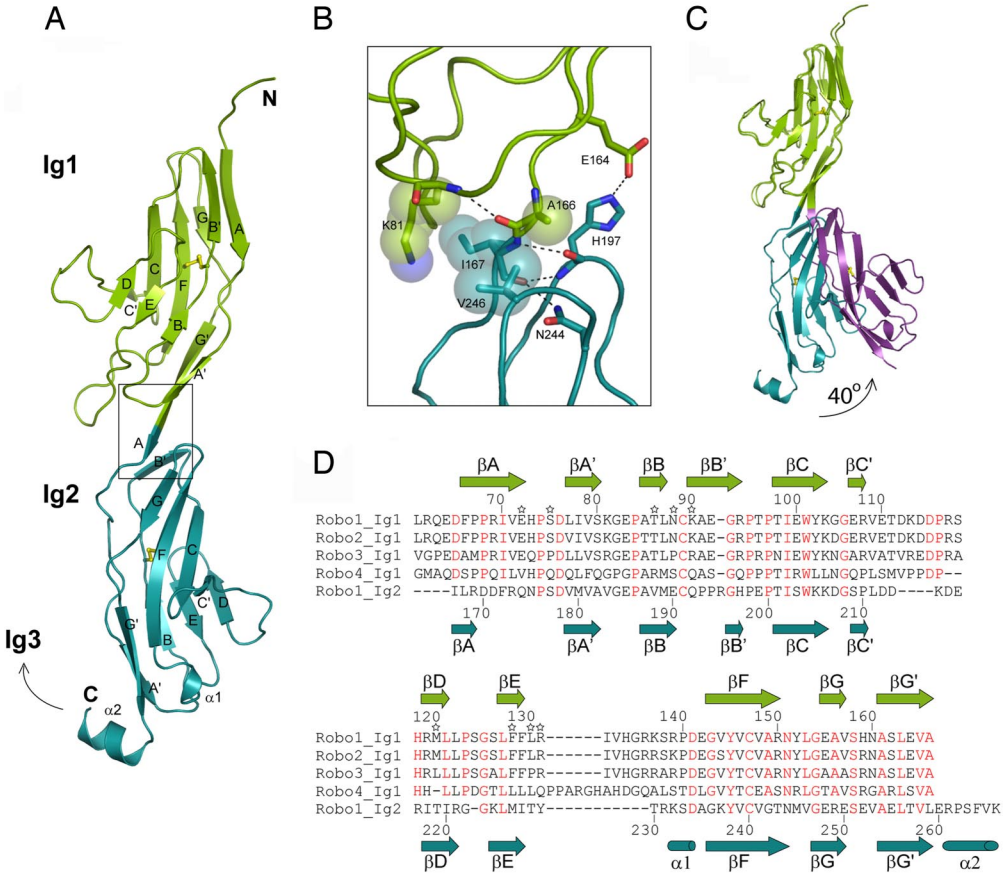

Fig. 1. Structure of human Robo1 Ig1–2. (*A*) Ribbon diagram. The disulfide bridges are in yellow, and the box indicates the region highlighted in *B*. (*B*) Residues involved in interdomain contacts of the Ig1-Ig2 interface. (*C*) Ribbon diagram of the two Ig1–2 crystal forms showing the hinge movement of Ig2. (*D*) Sequence alignment of Ig1 domains of human Robo1, -2, -3, and -4 and of the Ig2 domain of human Robo1. Residue numbering is for Robo1 Ig1 (above) and Robo1 Ig2 (below). Slit2 D2-binding residues selected for mutagenesis are marked with a star, and residues strictly conserved between the Ig1 domain of human Robo1, -2, -3, and -4 are shown in red.

contiguous with the first strand of Ig2 (βA), forming an extended module 100 Å long, with a pseudo-2-fold screw axis relating the two Ig domains (actual angle 172°).

The interdomain interface buries 610 Å^2 of surface area and involves four side chains (Lys-81, Ala-166, Ile-167, and Val-246), which make van der Waals contacts (Fig. 1*B*). In addition, Glu-164 in Ig1 forms a hydrogen bond with His-197 in Ig2. In a second crystal form, the elbow angle between the two domains is reduced from nearly 180° to 140° (actual change of 39.9°) (Fig. 1*C*), giving clear evidence for a flexible hinge between the two domains. This hinge motion eliminates the interdomain interface, but the hydrogen bond remains intact. Helix α2 at the C terminus of Robo1 Ig2 corresponds to the N terminus of the Ig3 domain. α2 makes a sharp turn that might allow Ig3 to pack against Ig2 and induce a U-shaped conformation of the Robo1 Ig1–4 domains, as observed for Ig1–4 from the chicken axonin-1 (24).

Structure of Slit2 D2. The 2.0-Å crystal structure of the isolated Slit2 D2 was solved by molecular replacement and reveals a canonical LRR fold, similar to the ectodomains of glycoprotein Ibα (25), the Nogo receptor (26), and the third LRR domain of *Drosophila* Slit (dSlit D3) (20). The domain's concave face is formed by eight β-strands, comprising a β-hairpin from the N-terminal cap and six parallel strands from the LRRs. Its convex face is formed by loops devoid of secondary structure, and the N- and C-terminal caps each contain two disulfide bridges [supporting information (SI) Fig. 4 *A* and *B*]. The four molecules in the asymmetric unit are nearly identical (rmsd$_{199C\alpha}$ < 0.45 Å) but display a dual conformation of the α1-β9 loop, corresponding to the "β-switch" loop of glycoprotein Ibα (25) (SI Fig. 4*C*). The dSlit D3 LRR is the closest structural neighbor to mammalian Slit2 D2 but is different in containing one less LRR.

Slit2 D2-Robo1 Ig-Binding Analysis. Slit binding, as measured in an *in vitro* pulldown assay, has been shown to require both the Ig1 and Ig2 domains from Robo1 (19). We analyzed the interaction of purified Slit2 D2 with Ig1–2 *in vitro* using surface plasmon resonance (SPR) spectroscopy and obtained a K_d value of ≈8 nM, in agreement with previous published data (20, 27–29) (Table 2). We then analyzed the Slit2 D2-binding affinity of the two individual Ig1 and Ig2 domains of Robo1 (Ig1, residues 61–166; and Ig2, residues 166–266) (Table 2). Compared with the Ig1–2 construct, the relative D2-binding capacity of Ig1 and Ig2 was 0.7 and 0.07, respectively. Determination of the kinetic constants yielded a K_d value of ≈8 nM for the Slit2 D2–Robo1 Ig1 interaction, similar to the K_d value obtained with Robo1 Ig1–2. The K_d value could not be determined for Robo1 Ig2, because it bound very weakly.

Structure of the Slit2 D2–Robo1 Ig1 Complex. We cocrystallized Slit2 D2 with Robo1 Ig1 and determined the structure at 1.7-Å resolution, whereas cocrystallization of Slit2 D2 with Ig1–2 failed to yield crystals. Consistent with mutagenesis studies (20), Robo1 Ig1 binds to the concave face of Slit2 D2, with the long axis of Ig1 at ≈60° to the longitudinal axis of D2 (Fig. 2*A*). Robo1 Ig1–Slit2 D2 complex

Table 1. Data collection and refinement statistics

	Ig1–2 rm	Ig 1–2 (Form 2)	Slit2 D2	Slit2 D2-Ig1
Data set				
Resolution, Å	30–2.5	30–2.0	30–2.0	30–1.7
Wavelength, Å	1.005	0.939	0.939	0.954
Completeness (outer shell), %	96.1 (80.1)	96.5 (88.3)	95.2 (93.4)	98.1 (94.9)
R_{merge}* (outer shell), %	5.2 (26.9)	6.4 (28.7)	11.6 (39.2)	8.2 (53.4)
Average $I/\sigma(I)$ (outer shell)	12.1 (3.1)	13.4 (4.3)	8.1 (4.0)	12.9 (2.5)
Refinement				
Reflections	9334	14074	60317	41951
R factor† (free R factor), %	22.7 (28.0)	25.8 (33.5)	21.3 (26.2)	18.6 (22.6)
rmsd bond, Å/angles, °	0.013/1.60	0.013/1.70	0.016/1.70	0.015/1.56

*$R_{merge} = \Sigma_{hkl}\Sigma_i |I_i(hkl) - \langle(hkl)\rangle|/|\Sigma_{hkl}\Sigma_i I_i(hkl)$.
†$R_{factor} = \Sigma_{hkl}||F_{obs}| - |F_{calc}||/\Sigma_{hkl}|F_{obs}|$.

formation does not introduce major rearrangements of the backbone of the uncomplexed domains ($rmsd_{106C\alpha}$ = 0.84 Å and $rmsd_{191C\alpha}$ = 0.40 Å, respectively). Complex formation buries 1,380 Å^2 of solvent-accessible surface area in an interface that consists of two distinct regions. The first region is predominantly electrostatic in nature and is formed by the β2-β3 loop and strands β3 and β4 of Slit2 D2 and the βA-βA′ and βB-βB′ loops of Ig1. Two salt bridges (involving Ig1 residues Glu-72 and Lys-90 and Slit2 D2 residues Arg-306 and Glu-304) and two hydrogen bonds (involving Asn-88 and Ser-75 of Ig1 and Arg-328 and Arg-287 of Slit2 D2) mediate direct contacts between the two proteins (Fig. 2*B*). Four water molecules make multiple bridging hydrogen bonds between Ig1 and D2 residues. The polar residues in this interface region display significant changes in side chain conformation upon complex formation (SI Fig. 5*A*).

The second contact region is predominantly hydrophobic and is formed by the packing of the βB-βE-βD cluster of Ig1 strands onto β6, β7, and β8 of Slit2 D2. It involves six Ig1 residues (Pro-84, Met-120, Leu-122, Phe-128, Leu-130, and Arg-131) and nine Slit2 D2 residues (Val-354, Ala-381, Leu-376, Leu-378, Leu-400, Ser-402, Tyr-404, His-426, and Ser-453) (Fig. 2*C*). This extensive apolar contact is reinforced by a hydrogen bond from Tyr-356 of Slit2 D2 to Thr-86 of Ig1. This interface is consistent with previous site-directed mutagenesis experiments performed with the *Drosophila* Slit, which showed that residues corresponding to Tyr-356, Leu-378, Tyr-404, and His-426 in human Slit2 were critical for Robo binding (20). Interestingly, most of the Robo1 Ig1 residues participating to the hydrophobic region of the Slit2 D2 interface are also involved in a homophilic interface burying 1,744 Å^2 of buried surface area within an antiparallel crystallographic dimer present in the first Robo1 Ig1–2 crystal form.

Mutagenesis Analysis of the Robo1 Ig1-Binding Site. We selected nine conserved Robo1 Ig1 residues from the complex interface for mutagenesis and analyzed their effect on wild-type Slit2 D2 binding using SPR. All mutations resulted in a significant loss of Slit2 D2 binding, except for the Ser75-Arg mutation, situated on the border of the interface (Fig. 2*D*). Disruption of the hydrogen bond between Thr-86 and Tyr-356 by the isosteric Thr-86-Val substitution was sufficient to reduce the Slit2 D2 binding by >50%. More dramatic effects on D2 binding were observed when the polar Asn-88 was replaced by a leucine or when the charges of Glu-72, Lys-90, and Arg-131 were reversed. Within the hydrophobic region of the interface, the substitution of Met-120, Phe-128, and Leu-130 by arginines reduced D2 binding by a factor of 6–20.

Table 2. Kinetic and dissociation constants and Slit2 D2-binding capacity of Robo1 constructs

Construct	Robo1 Ig1–2	Robo1 Ig1	Robo1 Ig2
K_{ar}, $M^{-1}s^{-1}$	5.5×10^5	4.4×10^5	ND
K_{dr}, s^{-1}	4.5×10^{-3}	3.5×10^{-3}	ND
$K_d = K_{dr}/K_{ar}$, nM	8.2	8.0	ND
Relative Slit2 D2 binding*	1	0.7	0.0

ND, not determined.
*The maximal Slit2 D2-binding capacity (R_{max}) of the constructs was normalized vs. the maximal Slit2 D2-binding capacity of Robo1 Ig.

Discussion

The Slit-Robo signaling complex acts as a key ligand–receptor interaction in the development of neurons, blood vessels, and some organs (1, 3, 5, 6). Although biochemical studies have defined the domains mediating Robo-Slit interaction as Robo Ig1–2 and Slit D2 (19, 20), many questions still remain. One important question is how the concave face of Slit D2 can bind two Ig domains when it is large enough only to accommodate a single Ig domain. Indeed, whereas some of the Slit D2 residues involved in complex formation are known, the molecular details of this interaction and the Robo residues involved are unknown. Another is exactly how heparin binding is integrated into the Slit-Robo signaling complex (21). Last, it is unknown how Slit binding to Robo is translated into a signal that is passed across the cellular membrane. The Robo1-Slit2 biochemical and structural data described here provide unique insights into these questions. The complex structure also expands the repertoire of Ig-binding regions currently known and is possibly useful in therapeutic drug design.

Robo Ig1 Sequence Comparison. Robo1, Robo2, and Robo3 all show specific high-affinity binding to Slit2 (15, 27), and our biochemical results provide conclusive evidence that the Robo1 Ig1 domain is the primary binding site for Slit2. A sequence alignment of metazoan homologues reveals that the Slit2 D2-binding residues are highly conserved (SI Fig. 6*A*), and that all but one of the Robo1-binding residues are invariant (SI Fig. 6*B*). The exception is Ser-75, which is not critical for Slit2 D2 binding in our SPR assay. This suggests that the interface observed in our structure is preserved in all metazoan Robo-Slit combinations, except those involving Robo4. In Robo4, many critical Slit2 binding residues are not present (e.g., Glu-72, Asn-88, Lys-90, Met-120, Phe-128, and Arg-131), consistent with the fact that no direct interaction between Robo4 and Slits has yet been observed.

Two human Robo3 isoforms, Robo3A and Robo3B, with very different biochemical properties have recently been identified (15). Robo3A differs from Robo3B by the insertion of 26 amino acids at its N terminus and was unable to bind Slit2 in an *in vitro* pulldown assay. The proximal location of this N-terminal extension to the

BIOCHEMISTRY

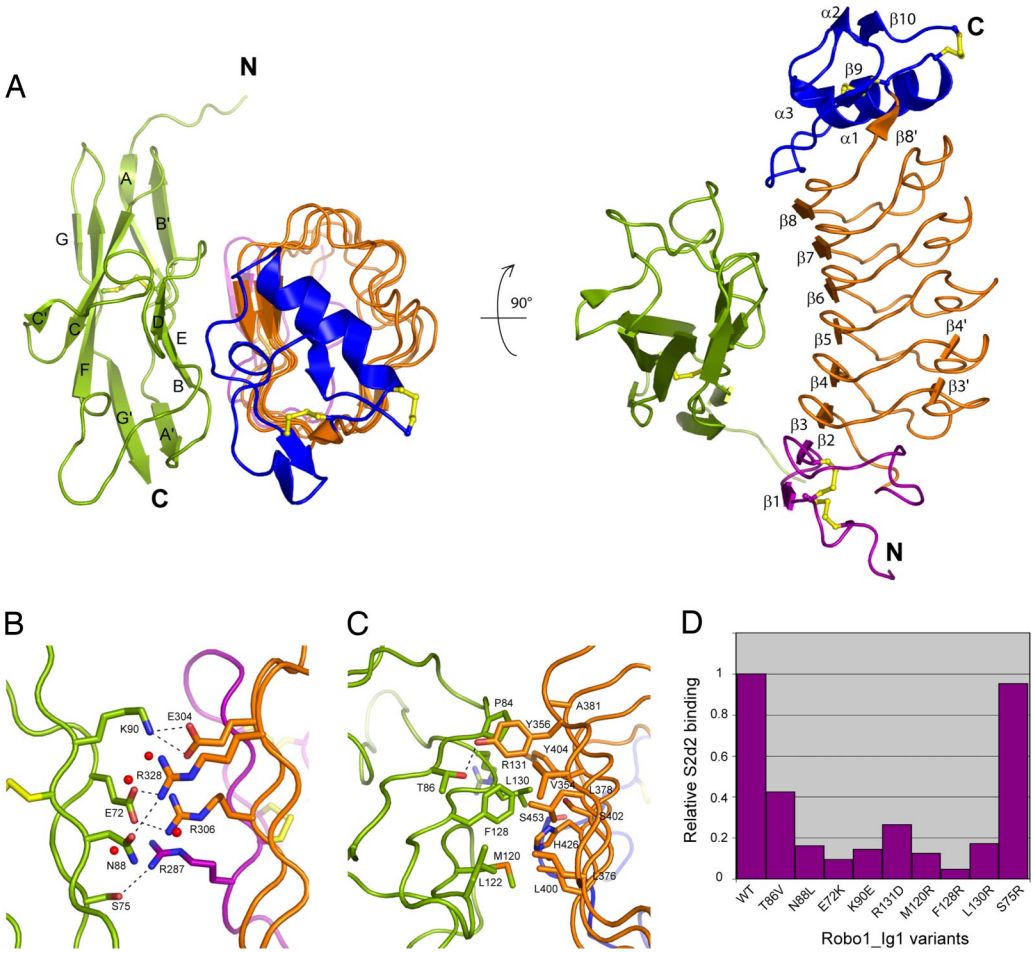

Fig. 2. Structure of Slit2 D2 bound to Robo1 Ig1. Ig1 is in green; Slit2 D2 N- and C-terminal caps are in purple and blue, respectively; LRRs 1–6 are in orange; and the disulfide bridges are in yellow. Interacting residues are shown in stick representation. (*A*) Ribbon diagram of the complex in two orthogonal orientations. (*B*) Electrostatic region of the Slit2 D2-Ig1 interface. (*C*) Hydrophobic region of the Slit2 D2-Ig1 interface. (*D*) Relative Slit2 D2-binding capacity of Robo1 Ig1 variants. Results are expressed as maximal Slit2 D2-binding, normalized with respect to the maximal Slit2 D2-binding capacity of wild-type Robo1 Ig1.

primary Slit2-binding region on Robo Ig1 suggests that the additional residues in Robo3A could shield the Slit2-binding site in this particular isoform. Whether this postulated shielding and the ability of Robo3A to heterophilically bind Robo1 (15) are of biological significance remains to be determined.

Heparin Binding. Heparin has recently been proposed to bind Slit2 D2 by means of a cluster of basic residues in the C-terminal cap, thereby enhancing the stability of the Slit2 D2-Robo1 Ig1–2 complex (21). Our structure shows that this putative heparin-binding site is still accessible in the complex (Fig. 3). Complex formation between FGF–FGF receptor (FGFR) is also heparin-dependent (30, 31). However, the heparin-binding site of the FGFR Ig2 domain (30, 31) involves a series of lysines corresponding to residues in Robo1 Ig1 that directly mediate Slit2 D2 recognition (Glu-72, Ser-75, Glu-83, Thr-86, and Asn-88). The heparin-binding site of Robo1 must therefore differ from that of FGFR in a ternary Slit2-Robo1–heparin complex.

Structural Implications for Signaling. An alignment of the Ig1 and Ig2 domains of human Robo1 involved in binding Slit2 (19) shows a high divergence of the Slit2-binding residues in Ig2, where few of the most important Slit2-binding residues are conserved (Fig. 1*D*). This observation, together with the 1:1 stoichiometric nature of the Slit2-Robo1 Ig1–2 complex (this work and ref. 21), does not support a Slit2 D2-Ig2 interface similar to that of Slit2 D2 with Ig1. Instead, as indicated by the poor binding affinity of Slit2 D2 for Ig2 revealed by our SPR experiments, we propose that Ig2 harbors a weak secondary Slit2 D2-binding site, which nevertheless appears to be required for Slit-Robo signaling (19). An intriguing possibility is that the flexibility of the Ig1-Ig2 linkage could allow Ig2 to simultaneously contact Slit2 D2 while it is primarily bound to Ig1 (Fig. 3), and that this could be part of the signal transduction mechanism.

Structure-Based Comparisons and Inhibitor Design. The Slit2-binding site of Robo1 differs from most other protein–protein interfaces involving an Ig domain in binding the ABB′ED sheet as opposed to the more frequently observed A′GG′FCC′ sheet interaction. The only other Ig domain known to mediate an interaction with this sheet is the Ig domain 5 of the tyrosine kinase receptor TrkA (TrkA Ig5) (32). Two regions on TrkA Ig5 mediate binding to nerve growth factor (NGF). The major region is from loops at the C-terminal pole, whereas the minor region involves the ABED sheet. Here, the N-terminal residues of NGF adopt a helical conformation and pack against the ABED sheet of TrkA Ig5 (32). Both the N-terminal NGF and TrkA Ig5 families share very little sequence conservation in these regions, and this is believed to be important for their ligand-receptor specificity (32). The ABB′ED sheet interface region of Robo1 Ig1, however, is significantly different from the

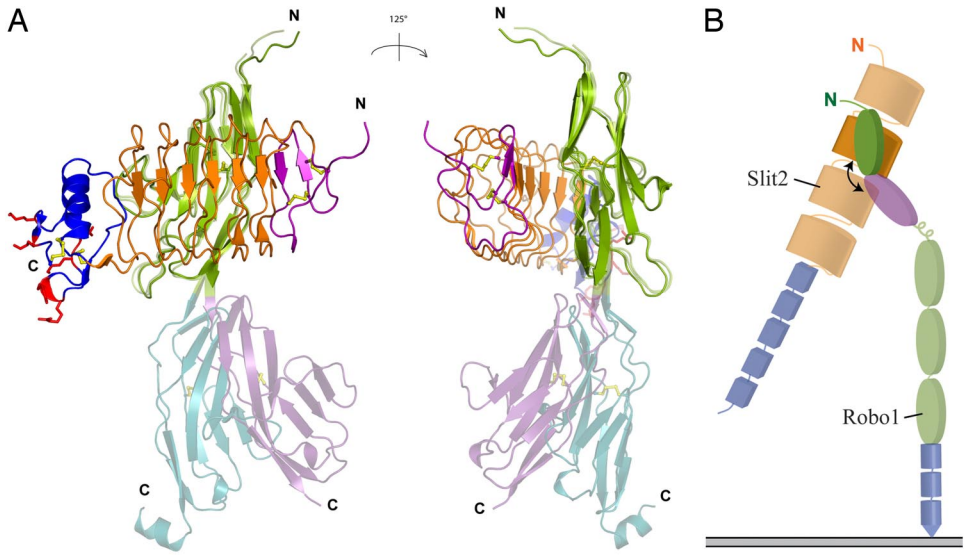

Fig. 3. Flexibility of the Robo1 Ig1-Ig2 linkage. (*A*) Superposition of the two Robo1 Ig1–2 crystal forms with the structure of Slit2 D2 bound to Robo1 Ig1, in two orientations. Ig1 is in green; Ig2 is in cyan or violet; Slit2 D2 N- and C-terminal caps are in purple and blue, respectively; LRRs 1–6 are in orange; and the disulfide bridges are in yellow. Slit2 D2 residues involved in heparin binding are in red and are shown in stick representation. (*B*) Schematic of the Slit2-Robo1 domain organization with the flexible linkage marked by a curved arrow. The Robo1 Ig1 domain is shown in green, and the Slit2 D2 is in orange. All other domains are opaque, the Robo1 Ig2 is in magenta, the other Ig domains are in green, and the FN3 domains are in blue. The Slit2 LRR domains are colored in orange, and the EGF domains are in blue.

TrkA Ig5-binding region in being highly conserved and much more extensive.

The Slit2 D2-Robo1 Ig1 complex presented here represents a previously undescribed interaction of an LRR domain with an Ig domain and once again illustrates the enormous versatility of Ig domains in mediating protein–protein interactions (33). This unique interaction region therefore provides an attractive target for the rational design of specific Slit-Robo signaling inhibitors. Here, the extended N-terminal peptide of Robo3A, which blocks Slit2 binding, may provide a useful lead in a structure-based design approach. Such inhibitors would have applications in antiangiogenic therapy (4) or in blocking Slit-Robo-mediated cancer cell metastasis (7).

Materials and Methods

Preparation and Crystallization of Recombinant Proteins. We subcloned Robo1 Ig1 and Robo1 Ig2 cDNA into a modified pTT3 expression vector (34) encoding a secretion signal peptide followed by a hexa-histidine tag. Robo1 Ig1 point mutants were generated by using the QuikChange kit (Stratagene, La Jolla, CA). Proteins were expressed and purified as described (35). The human Robo1 construct encompassing the first two Ig domains (residues 61–268) and the second LRR domain of human Slit2 (residues 271–479) were crystallized as described (22, 35). Crystals of the Slit2 D2-Robo1 Ig1 complex were grown at 20°C by the hanging-drop method. Two microliters of a protein solution containing an equimolar ratio of Slit2 D2 and Robo1 Ig1 was mixed with 1 μl of reservoir solution containing 12% PEG 6000, 0.1 M Li_2SO_4, and 0.1 M citrate, pH 5.6. The crystals belong to space group $P2_12_12$ with unit-cell dimensions a = 51.3 Å, b = 190.1 Å, and c = 40.9 Å and contain one complex per asymmetric unit.

Phasing and Refinement. Diffraction data were collected at ID14-4 of the European Synchrotron Radiation Facility at two different wavelengths near the Hg L-III absorption edge from a single Robo1 Ig1–2 crystal soaked in Hg acetate. The positions of two Hg atoms in the asymmetric unit were determined with SHELXD (36), and the phases were calculated and improved by using SHARP (37) (SI Table 3). The structure was refined at 2.5 Å against data collected at the remote wavelength. The second crystal form of Robo1 Ig1–2 was solved by molecular replacement by using the individual Ig1 and Ig2 domains from crystal form 1 and refined to 2-Å resolution. The R and R_{free} values for this crystal form 2 are larger than expected, and this is probably due to the presence of a weak super lattice observed in the diffraction pattern, indicative of some kind of translational disorder that we have not been able to model. The Slit2 D2-Robo1 Ig1 complex was solved at 1.7 Å by molecular replacement (38) using human Slit2 D3 (22) and human Robo1 Ig1 structures. The Slit2 D2 structure was determined at 2 Å by molecular replacement (38) by using the structure of the LRR domain from Slit2 D2-Robo1 Ig1 complex. The diffraction data were reduced by using XDS (39), and the crystallographic models were refined by using CCP4 programs (38) iterated with manual rebuilding. A summary of the refinement statistics is given in Table 1.

SPR Spectroscopy. Analyses were performed by using a BIAcore 3000 instrument (BIAcore AB, Uppsala, Sweden). Robo1 constructs were immobilized (400–1,000 resonance units) on the surface of a CM5 sensor chip (BIAcore) using the amine-coupling chemistry (Biacore amine coupling kit) according to the manufacturer's instructions. Binding of Slit2 D2 was measured at a flow rate of 20 μl per min in 145 mM NaCl/10 mM Hepes (pH 7.4), containing 0.005% surfactant P20 (BIAcore). Equivalent volumes of each protein sample were injected over a surface with no protein immobilized to serve as blank sensorgrams for subtraction of the bulk refractive index background. Regeneration of the surfaces was achieved by injection of 20 μl of 2 M NaCl. Data were analyzed by global fitting to a 1:1 Langmuir-binding model of the association and dissociation phases for several concentrations simultaneously using the BIAevaluation 3.1 software (BIAcore AB). The apparent equilibrium dissociation constants (K_d) were calculated from the ratio of the dissociation K_{dr} and association K_{ar} rate constants, and maximal binding capacities (R_{max}) were determined by using the same model.

We thank C. Petosa for critically reading this manuscript. We gratefully acknowledge the use of the European Molecular Biology Laboratory (EMBL), Grenoble, high-throughput crystallization facility, and we thank the EMBL–Grenoble/European Synchrotron Radiation Facility (ESRF) Joint Structural Biology Group for access and support at ESRF beamlines ID14-4 and ID23-1. Partial funding for this project was provided by the European Commission Framework 6 Integrated Project "SPINE2-Complexes."

1. Dickson BJ, Gilestro GF (2006) *Annu Rev Cell Dev Biol* 22:651–675.
2. Garbe DS, Bashaw GJ (2004) *Crit Rev Biochem Mol Biol* 39:319–341.
3. Carmeliet P, Tessier-Lavigne M (2005) *Nature* 436:193–200.
4. Fujiwara M, Ghazizadeh M, Kawanami O (2006) *Vasc Med* 11:115–121.
5. Qian L, Liu J, Bodmer R (2005) *Curr Biol* 15:2271–2278.
6. Santiago-Martinez E, Soplop NH, Kramer SG (2006) *Proc Natl Acad Sci USA* 103:12441–12446.
7. Prasad A, Fernandis AZ, Rao Y, Ganju RK (2004) *J Biol Chem* 279:9115–9124.
8. Ito H, Funahashi S, Yamauchi N, Shibahara J, Midorikawa Y, Kawai S, Kinoshita Y, Watanabe A, Hippo Y, Ohtomo T, *et al.* (2006) *Clin Cancer Res* 12:3257–3264.
9. Itoh A, Miyabayashi T, Ohno M, Sakano S (1998) *Brain Res Mol Brain Res* 62:175–186.
10. Kidd T, Brose K, Mitchell KJ, Fetter RD, Tessier-Lavigne M, Goodman CS, Tear G (1998) *Cell* 92:205–215.
11. Huminiecki L, Gorn M, Suchting S, Poulsom R, Bicknell R (2002) *Genomics* 79:547–552.
12. Park KW, Morrison CM, Sorensen LK, Jones CA, Rao Y, Chien CB, Wu JY, Urness LD, Li DY (2003) *Dev Biol* 261:251–267.
13. Stein E, Tessier-Lavigne M (2001) *Science* 291:1928–1938.
14. Sabatier C, Plump AS, Le M, Brose K, Tamada A, Murakami F, Lee EY, Tessier-Lavigne M (2004) *Cell* 117:157–169.
15. Camurri L, Mambetisaeva E, Davies D, Parnavelas J, Sundaresan V, Andrews W (2005) *Mol Cell Neurosci* 30:485–493.
16. Rothberg JM, Artavanis-Tsakonas S (1992) *J Mol Biol* 227:367–370.
17. Wang KH, Brose K, Arnott D, Kidd T, Goodman CS, Henzel W, Tessier-Lavigne M (1999) *Cell* 96:771–784.
18. Sundaresan V, Roberts I, Bateman A, Bankier A, Sheppard M, Hobbs C, Xiong J, Minna J, Latif F, Lerman M, Rabbitts P (1998) *Mol Cell Neurosci* 11:29–35.
19. Liu Z, Patel K, Schmidt H, Andrews W, Pini A, Sundaresan V (2004) *Mol Cell Neurosci* 26:232–240.
20. Howitt JA, Clout NJ, Hohenester E (2004) *EMBO J* 23:4406–4412.
21. Hussain SA, Piper M, Fukuhara N, Strochlic L, Cho G, Howitt JA, Ahmed Y, Powell AK, Turnbull JE, Holt CE, Hohenester E (2006) *J Biol Chem* 281:39693–39698.
22. Morlot C, Hemrika W, Romijn RA, Gros P, Cusack S, Mc Carthy AA (2007) *Acta Crystallogr D* 63:961–968.
23. Casasnovas JM, Stehle T, Liu JH, Wang JH, Springer TA (1998) *Proc Natl Acad Sci USA* 95:4134–4139.
24. Freigang J, Proba K, Leder L, Diederichs K, Sonderegger P, Welte W (2000) *Cell* 101:425–433.
25. Huizinga EG, Tsuji S, Romijn RA, Schiphorst ME, de Groot PG, Sixma JJ, Gros P (2002) *Science* 297:1176–1179.
26. He XL, Bazan JF, McDermott G, Park JB, Wang K, Tessier-Lavigne M, He Z, Garcia KC (2003) *Neuron* 38:177–185.
27. Brose K, Bland KS, Wang KH, Arnott D, Henzel W, Goodman CS, Tessier-Lavigne M, Kidd T (1999) *Cell* 96:795–806.
28. Nguyen Ba-Charvet KT, Brose K, Ma L, Wang KH, Marillat V, Sotelo C, Tessier-Lavigne M, Chedotal A (2001) *J Neurosci* 21:4281–4289.
29. Li HS, Chen JH, Wu W, Fagaly T, Zhou L, Yuan W, Dupuis S, Jiang ZH, Nash W, Gick C, *et al.* (1999) *Cell* 96:807–818.
30. Pellegrini L, Burke DF, von Delft F, Mulloy B, Blundell TL (2000) *Nature* 407:1029–1034.
31. Schlessinger J, Plotnikov AN, Ibrahimi OA, Eliseenkova AV, Yeh BK, Yayon A, Linhardt RJ, Mohammadi M (2000) *Mol Cell* 6:743–750.
32. Wiesmann C, Ultsch MH, Bass SH, de Vos AM (1999) *Nature* 401:184–188.
33. Wiesmann C, Muller YA, de Vos AM (2000) *J Mol Med* 78:247–260.
34. Durocher Y, Perret S, Kamen A (2002) *Nucleic Acids Res* 30:E9.
35. Morlot C, Hemrika W, Romijn RA, Gros P, Cusack S, McCarthy AA (2007) *Acta Crystallogr F* 63:689–691.
36. Schneider TR, Sheldrick GM (2002) *Acta Crystallogr D* 58:1772–1779.
37. La Fortanelle ED, Bricogne G (1997) *Methods Enzymol* 276:472–494.
38. Collaborative Computational Project N (1994) *Acta Crystallogr D* 50:760–763.
39. Kabsch W (1993) *J Appl Crystallogr* 26:795–800.